Journal of Applied Polymer Science

Effect of copper sulfate pentahydrate on the structure and properties of poly(vinyl alcohol)/graphene oxide composite films

Qian Liu,[1] Xiang Ge,[1] Aimin Xiang,[1] Huafeng Tian[1,2]

[1]School of Material and Mechanical Engineering, Beijing Technology and Business University, Beijing 100048, China

[2]Key Laboratory of Carbohydrate and Biotechnology (Ministry of Education), Jiangnan University, Lihu Road 1800, Wuxi 214122, China

Correspondence to: H. Tian (E-mail: tianhuafeng@th.btbu.edu.cn)

ABSTRACT: Poly(vinyl alcohol) (PVA)/graphene oxide (GO)/copper sulfate pentahydrate ($CuSO_4{\cdot}5H_2O$) composite films were prepared by the solution casting method, and the effect of $CuSO_4{\cdot}5H_2O$ on the structure and properties of the PVA/GO composites was investigated. Fourier transform infrared (FTIR) analysis proved the crosslinking interaction between $CuSO_4{\cdot}5H_2O$ and the —OH group of PVA. The crystallinity of the composite films increased first and then decreased. For the composite films, the tensile strength, Young's modulus, and yield stress values improved with increasing $CuSO_4{\cdot}5H_2O$, whereas the elongation at break decreased compared with that of the neat PVA/GO composite film. The thermogravimetric analysis (TGA) and derivative thermogravimetry (DTG) patterns of the PVA/GO/$CuSO_4{\cdot}5H_2O$ composite films showed that the thermal stability decreased; this was consistent with the TGA–FTIR analysis. A remarkable improvement in the oxygen-barrier properties was achieved. The oxygen permeability coefficient was reduced by 60% compared to that of the neat PVA/GO composite film. © 2016 Wiley Periodicals, Inc. J. Appl. Polym. Sci. **2016**, *133*, 44135.

KEYWORDS: crosslinking; mechanical properties; membranes; properties and characterization; thermal properties

Received 18 November 2015; accepted 22 June 2016

DOI: 10.1002/app.44135

INTRODUCTION

Recent progress in biotechnology and nanotechnology has led to the expansion of a rich variety of novel materials, precisely manufactured at the nanoscale level, with great potential to improve traditional scientific research.[1] The expansion of nanotechnology into different areas has generated a demand for research on new materials that have optimized properties.[2] Among these materials, graphene oxide (GO) has exhibited increasing technological significance, with widespread applications in the fields of biomedical and biodegradable material. During the last half decade, a two-dimensional single sheet of GO has attracted a great deal of interest because of its low cost, unique structure, and favorable properties. GO can be prepared on a large scale from low-cost natural graphite, which is an easily available material.[3–5] The presence of oxygen functional groups, such as hydroxyl, carboxyl, carbonyl, and epoxide groups, facilitate the dispersion of GO sheets in polar solvents. Moreover, the functional groups in the GO sheets impart strong interactions with polar molecules or polymers to form GO-intercalated composites.[6–8] This offers the possibility of making multifunctional nanocomposites in a cost-effective way over other expensive fillers such as carbon nanotubes. There have been several reports on GO/polymer nanocomposites with significant improvements in the thermal, mechanical, and gas-barrier properties. Wang *et al.*[9] studied the curing dynamics and network formation of cyanate ester resin/GO nanocomposites. The incorporation of GO into the resin matrix showed a strong catalytic effect on the curing of the resin, and the addition of 4% GO resulted in a decrease of the curing temperature to 97 °C.

Poly(vinyl alcohol) (PVA) is a water-soluble, biocompatible, and degradable polymer, and it has been applied in a variety of fields.[10–12] For its excellent film-forming ability, PVA has been widely used in film industrial production and scientific research. There are massive hydroxyl groups on the main chain of PVA.[13] However, the pure PVA shows some drawbacks, such as a low elastic modulus, poor abrasion resistance, and severe creep problem; this leads to the early failure of pure PVA and restricts its use in industry.[14–17] To overcome the aforementioned drawbacks, the addition of a small fraction of nanosize particles, such as nanoclay, carbon nanotubes, or GO,[18–21] have shown great successes in industrial applications, and this has attracted considerable fundamental academic interests because of reported dramatic improvements in the mechanical strength.[22–26]

In our earlier article,[27] we reported the effect of GO on the structure and properties of PVA composite films with significant

improvements in the thermal, mechanical, and gas-barrier properties. To further increase the mechanical properties of PVA/GO composites, PVA was crosslinked with inorganic metal ions, copper sulfate pentahydrate ($CuSO_4{\cdot}5H_2O$), in this study. The effect of the $CuSO_4{\cdot}5H_2O$ content on the structure and properties of the PVA/GO/$CuSO_4{\cdot}5H_2O$ composite films were investigated in detail. In this study, we expected to obtain ecofriendly PVA/GO/$CuSO_4{\cdot}5H_2O$ composite films with excellent mechanical, thermal, and gas-barrier properties; this could promote the application of PVA in the packaging industry.

EXPERIMENTAL

Materials

PVA (99 mol % hydrolyzed, degree of polymerization = 1700) was purchased from Kuraray Co., Ltd. Natural graphite powder, hydrogen peroxide (H_2O_2), sodium nitrate ($NaNO_3$), $CuSO_4{\cdot}5H_2O$, and glycerol were purchased from Sinopharm Chemical Reagent Beijing Co., Ltd. Concentrated sulfuric acid (H_2SO_4), potassium permanganate ($KMnO_4$), and hydrochloric acid (HCl) were obtained from Beijing Chemical Works. All of these materials were used directly without further purification.

GO Preparation

According to the traditional Hummers method, GO was prepared from natural graphite powder by the oxidation with $KMnO_4$ in concentrated H_2SO_4. Natural graphite powder (2 g) and $NaNO_3$ (1 g) were added to concentrated H_2SO_4 (46 mL). The mixture was stirred uniformly under an ice bath. Then, $KMnO_4$ (6 g) was added gradually to the mixture. Two hours later, the mixture was heated up to 35 °C and maintained there for 30 min. A certain amount of deionized water was added slowly to the mixture. Then, the mixture was heated up to 98 °C and stirred for another 20 min. The final mixture was filtered and washed successively with an HCl aqueous solution and distilled water until the pH reached 7–8. After sonication and dialysis of the GO solution, the final GO powder sample was obtained by vacuum freeze drying.

PVA/GO/$CuSO_4{\cdot}5H_2O$ Composite Film Preparation

A 5 wt % PVA solution with glycerol plasticizer (10 wt % of PVA) was prepared by the dissolution of PVA in deionized water at 90 °C. GO was dispersed in the distilled water by ultrasonication. The GO aqueous dispersion (5 wt %) was added gradually into the PVA solution and stirred for 30 min. Then, $CuSO_4{\cdot}5H_2O$ as a crosslinker in the desired amount was added to the PVA solution and stirred for 30 min. The mixture was immediately subjected to sonication at room temperature to obtain a uniform dispersion. Then, the homogeneous solution was poured onto glass plates and dried at room temperature to obtain the PVA/GO/$CuSO_4{\cdot}5H_2O$ composite film. The GO content was fixed at 5% for all the samples.

Characterization

The rheological measurements were conducted on a Haake HR parallel-plate rheometer equipped with a parallel-plate geometry with plates 20 mm in diameter. All measurements were performed in the dynamic mode with a gap of 1.0 mm. The samples were placed in the rheometer and allowed to equilibrate for 1 min. The parallel plates were then moved to a gap of 1.0 mm, and the excess polymer was trimmed. Samples were measured under a nitrogen blanket to prevent degradation. Strain sweeps were performed before the frequency sweeps to establish the linear region. A frequency range of 10 s^{-1} was investigated with a variable strain method. This method entailed the use of the maximum strain within the linear region.

Fourier transform infrared (FTIR) spectra of the polymer were recorded in the region 4000–400 cm^{-1} with a resolution of 4 cm^{-1} on a Nicolet iN10 MX device spectrometer (Thermo Fisher Scientific).

X-ray diffraction (XRD) measurements were performed directly on the samples with a Rigaku D-Max-2500 VB2+/pc device (40 kV, 40 mA, Rigaku Co, Japan) with Cu irradiation at a scanning rate of 10°/min in the 2θ range 5–40°.

The mechanical properties of the membranes were analyzed with a testing machine (MTS systems China Co., Ltd.) in tensile mode according to ASTM D 638 at room temperature with an extension speed of 20 mm/min and an initial gauge length of 40 mm. The samples were conditioned at a relative humidity of 35% for 2 days before testing. The data reported were averaged over at least five specimens.

Thermogravimetric analysis (TGA) of the composite films were performed with a thermogravimetric analyzer Q5000IR (TA Instruments). After the samples (5 mg) were weighed in a pan, they were placed inside a tube furnace, which was heated up from 35 to 800 °C at a rate of 20 °C/min under a nitrogen atmosphere.

TGA was carried out via a thermogravimetric analyzer (209 F1, Netzsch, Germany) at a linear heating rate of 20 °C/min under a nitrogen atmosphere. The temperature range was from 35 to 800 °C. The thermogravimetry was coupled with TGA–FTIR investigations with a Nicolet 6700 spectrophotometer (Thermo Scientific). The volatile gas produced from thermal decomposition was analyzed online by FTIR spectroscopy with samples of about 10 mg.

The oxygen permeability of the composite films was measured with a BT-3 device (Toyoseiki Japan Co., Ltd.). The test operating conditions temperature was 25 °C and the relative humidity was 75%. The test was based on the principle of using the partial pressure difference of oxygen among the film sample. The pressure of the upper cell was set at 100 kPa, whereas the opposite was set as the vacuum. With progressing time, the oxygen gas began to penetrate the sample film, and the information of the relative gas pressure was recorded. All of the gas permeation data presented were the average of three replicate acetate measurements.

RESULTS AND DISCUSSION

Shear Viscosity

To study the crosslinking effect of Cu^{2+}, the shear viscosity of the PVA/GO/$CuSO_4{\cdot}5H_2O$ solution was measured, as shown in Figure 1. With the increase of $CuSO_4{\cdot}5H_2O$ in the PVA/GO/$CuSO_4{\cdot}5H_2O$ solution, the shear viscosity increased from 18.5 mPa s for the PVA/GO solution without $CuSO_4{\cdot}5H_2O$ to 20.8mPa s for the PVA/GO/$CuSO_4{\cdot}5H_2O$ solution with 9%

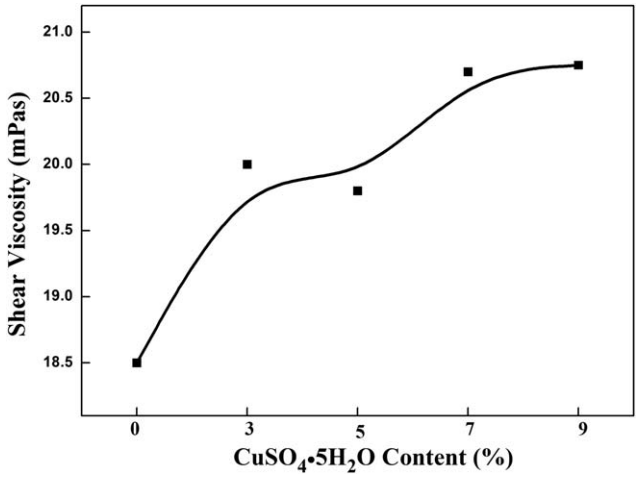

Figure 1. Shear viscosity of the PVA/GO/$CuSO_4{\cdot}5H_2O$ solution.

$CuSO_4{\cdot}5H_2O$. After Cu^{2+} ions were introduced into the PVA solution, intermolecular and/or intramolecular crosslinking between $Cu^{2+}$and the PVA chains may have formed. The —OH group of PVA had strong complexation ability to transition-metal ions.[28,29] The increase of the shear viscosity was attributed to the crosslinking effect in the form of coordination bonds between the Cu^{2+} and the —OH group of PVA.

FTIR Analysis

The FTIR spectra of the PVA/GO/$CuSO_4{\cdot}5H_2O$ composite films are shown in Figure 2. For the PVA/GO composite film without $CuSO_4{\cdot}5H_2O$, the broad peak at 3430 cm^{-1} was assigned to the stretching vibrations of hydroxyl groups (—OH). With the incorporation of $CuSO_4{\cdot}5H_2O$, no new absorption peaks appeared in the spectra; this suggested that no new functional groups were formed during the preparation process of the PVA/GO/$CuSO_4{\cdot}5H_2O$ composite films. With increasing $CuSO_4{\cdot}5H_2O$, the characteristic peak of the PVA/GO composite films at 3430 cm^{-1} corresponding to the —OH group gradually shifted to 3380 cm^{-1}. After the introduction of Cu^{2+} ions into PVA, intermolecular and/or intramolecular crosslinking between Cu^{2+} and PVA chains formed. As result, the redshift of functional groups was attributed to the crosslinking of hydroxyl groups on the PVA/GO composite film with Cu^{2+} ions.

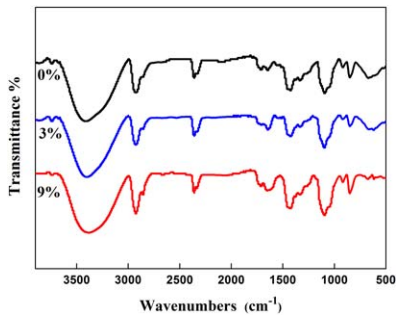

Figure 2. FTIR curves for the PVA/GO/$CuSO_4{\cdot}5H_2O$ composite films. [Color figure can be viewed in the online issue, which is available at wileyonlinelibrary.com.]

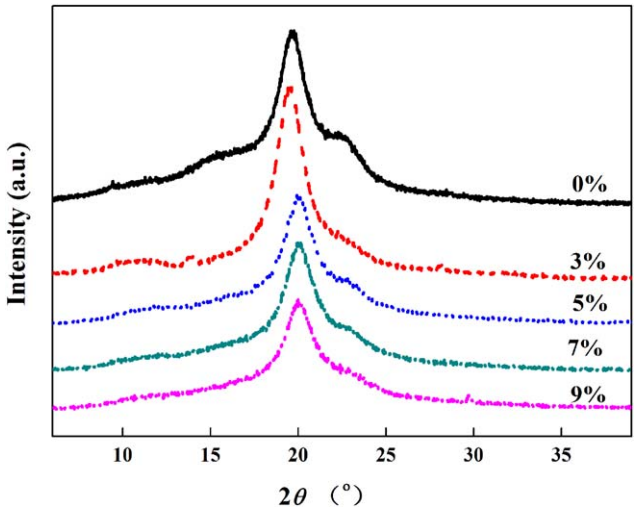

Figure 3. XRD curves for the PVA/GO/$CuSO_4{\cdot}5H_2O$ composite films. [Color figure can be viewed in the online issue, which is available at wileyonlinelibrary.com.]

XRD Analysis

Figure 3 shows the XRD patterns of the PVA/GO/$CuSO_4{\cdot}5H_2O$ composite films with different amounts of $CuSO_4{\cdot}5H_2O$. The PVA/GO film without $CuSO_4{\cdot}5H_2O$ exhibited two diffraction peaks at 20.07 and 21.96°; these peaks corresponded to the 101 and 200 crystal planes, respectively, of PVA. The characteristic peak of GO at a 2θ of 11.9° did not appear; this indicated that GO was well dispersed in the PVA matrix. With the addition of $CuSO_4{\cdot}5H_2O$, no new diffraction peaks were observed, and the location of two diffraction peaks did not change either; this indicated that the crystal type of the PVA/GO/$CuSO_4{\cdot}5H_2O$ composite films remained the same as that of the PVA matrix. The crystallinity of the composite film was calculated and is shown in Figure 4. PVA was partially crystalline and consisted of crystalline layers or lamellas and folded chains joined together by tie molecules, which formed amorphous regions between the lamellas. The crystallinity increased obviously with the

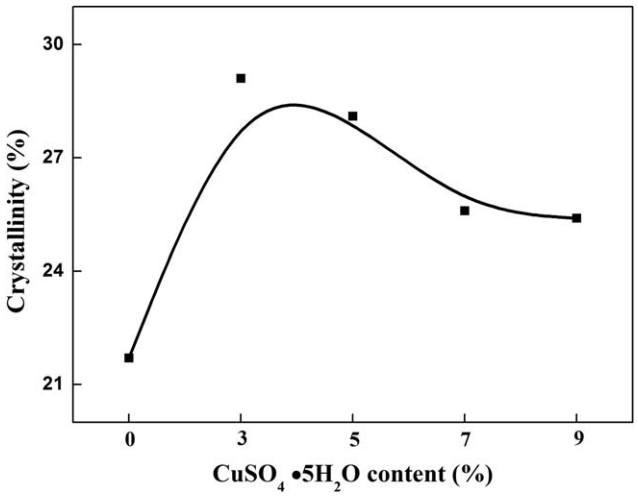

Figure 4. Crystallinity of the PVA/GO/$CuSO_4{\cdot}5H_2O$ composite films with respect to the $CuSO_4{\cdot}5H_2O$ content.

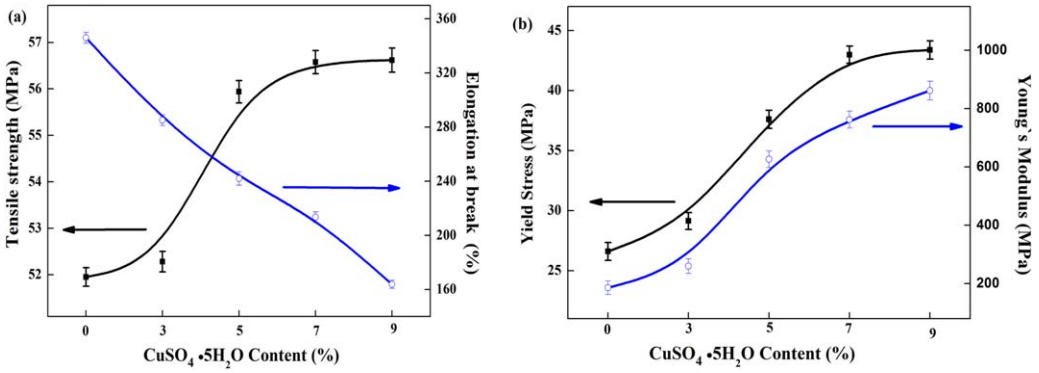

Figure 5. Mechanical properties of the PVA/GO/$CuSO_4{\cdot}5H_2O$ composite films: (a) tensile strength and elongation at break and (b) yield stress and Young's modulus. [Color figure can be viewed in the online issue, which is available at wileyonlinelibrary.com.]

increasing $CuSO_4{\cdot}5H_2O$ and reached a maximum at 3% $CuSO_4{\cdot}5H_2O$. The crystallinity began to decrease with a further increase in $CuSO_4{\cdot}5H_2O$. There were two factors affecting the crystallization behavior. The first was the weakening of the hydrogen bonds between PVA molecules due to the formation of complexation bonds between —OH and Cu^{2+}; this promoted crystallization behavior. The second factor was the crosslinking effect of the interaction between PVA and Cu^{2+} ions; this decreased the crystallization ability and resulted in a decrease in the crystallinity.

Mechanical Properties

The mechanical properties of the PVA/GO/$CuSO_4{\cdot}5H_2O$ composite films with different $CuSO_4{\cdot}5H_2O$ contents are shown in Figure 5. The PVA/GO composite film without $CuSO_4{\cdot}5H_2O$ exhibited flexible characteristics with a high elongation at break and a low tensile strength, yield stress, and Young's modulus. The introduction of $CuSO_4{\cdot}5H_2O$ into PVA/GO greatly improved the mechanical properties of the PVA/GO composite film. With increasing $CuSO_4{\cdot}5H_2O$ in the composite films, the tensile strength increased from 51.9 MPa in the composite film without $CuSO_4{\cdot}5H_2O$ to 56.6 MPa of the composite film with 9% $CuSO_4{\cdot}5H_2O$. The Young's modulus achieved a significant enhancement of 363% over that of the composite film without $CuSO_4{\cdot}5H_2O$. The yield stress increased from 26.6 MPa for the composite film without $CuSO_4{\cdot}5H_2O$ to 43.4 MPa. Although the corresponding elongation at break of the PVA/GO/$CuSO_4{\cdot}5H_2O$ composite films decreased with increasing $CuSO_4{\cdot}5H_2O$. The introduction of $CuSO_4{\cdot}5H_2O$ exhibited a dramatic crosslinking effect with strong intermolecular /intramolecular interactions between PVA and Cu^{2+} in the PVA/GO composite film; this decreased the mobility of the polymer segment. The crystallinity increment of PVA by $CuSO_4{\cdot}5H_2O$ also contributed to the enhancement of the mechanical performance of the composite films, as indicated in the XRD section.

Thermal Stability

The thermal properties represent one of the most important properties in polymer nanocomposites. Thus, the thermal stability of the PVA/GO/$CuSO_4{\cdot}5H_2O$ composite films were investigated with TGA, and the weight loss traces recorded in the temperature range 35–800 °C are shown in Figure 6. According to these curves, the thermal decomposition of the PVA/GO composite films without $CuSO_4{\cdot}5H_2O$ could be divided into three segments. For the first segment around 200–278 °C, the mass loss was mainly due to the release of the plasticizer present in PVA and the pyrolysis of the labile oxygen-containing functional groups on GO in the forms of CO and CO_2. For the second segment around 330 °C, the mass loss was attributed to the elimination of residual acetate groups, which were on the PVA for the incomplete alcoholysis of poly(vinyl acetate). For the third segment around 450 °C, the mass loss was attributed to

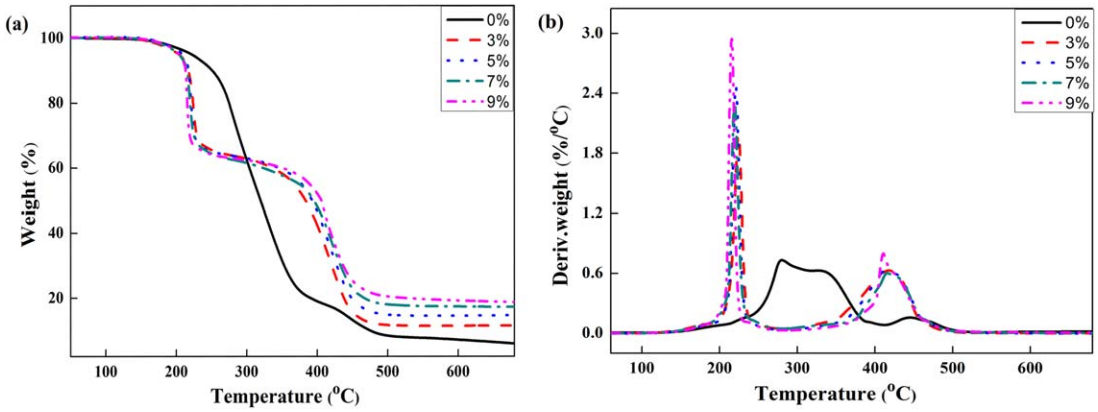

Figure 6. (a) TGA and (b) DTG curves for the PVA/GO/$CuSO_4{\cdot}5H_2O$ composite films. [Color figure can be viewed in the online issue, which is available at wileyonlinelibrary.com.]

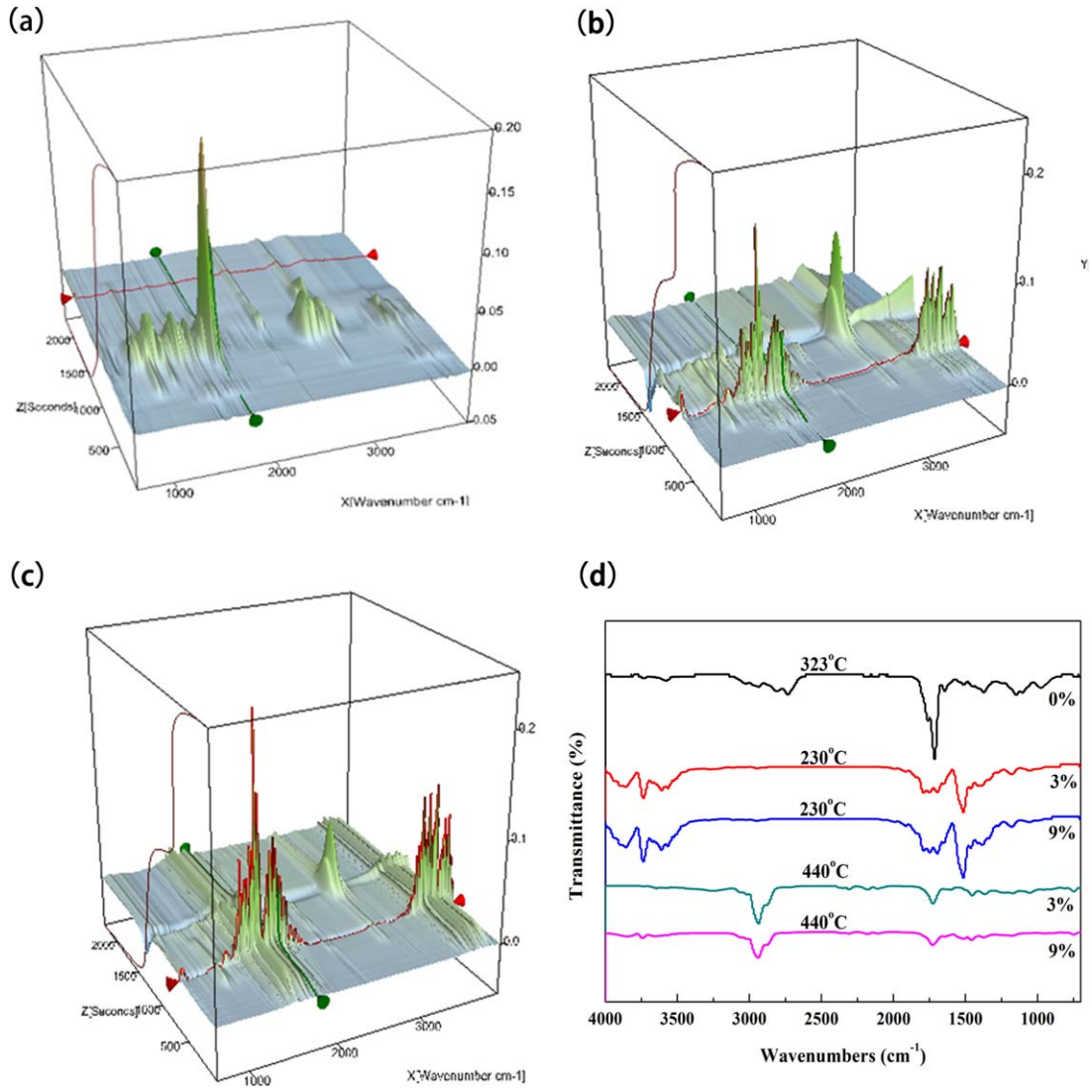

Figure 7. TGA–FTIR curves for the PVA/GO/$CuSO_4{\cdot}5H_2O$ composite films. [Color figure can be viewed in the online issue, which is available at wileyonlinelibrary.com.]

the breakdown of the polymer backbone. The decomposition rate of the acetate group was much higher than the decomposition of the polymer backbone. With the introduction of $CuSO_4{\cdot}5H_2O$, the residual carbon of the samples significantly decreased in the range 200–330 °C, and the decomposition temperature (Td) corresponding to the maximum thermal decomposition rate from the derivative DTG curves gradually decreased. This indicated a decreasing thermal stability in the composite film. Although the PVA/GO/$CuSO_4{\cdot}5H_2O$ composite films exhibited an obvious improvement in the thermal stability in the range 400–500 °C, with increasing $CuSO_4{\cdot}5H_2O$, the residual carbon of the composite films increased significantly from 15% for the neat PVA/GO composite film to 32% for the composite film with 9% $CuSO_4{\cdot}5H_2O$. TGA showed that the thermal stability of the PVA/GO composite films after crosslinking was changed.

To further investigate the thermal stability, a coupled TGA–FTIR study used as the online analysis of the evolved gases was performed (Figure 7). In the application of the TGA–FTIR system, the TGA instrument provided thermal extraction, and the FTIR instrument served as a detector. For the PVA/GO composite films, the maximum heat loss rate was at about 323 °C. The peaks at 2720 and 2820 cm^{-1} were assigned to the stretching vibrations of C—H. The absorption peak at 1740 cm^{-1} was attributed to the stretching vibrations of C═O. The peaks at 1370 and 1150 cm^{-1} were assigned to the stretching vibrations of C—O and C—C. The results conclusively demonstrated that the maximum heat loss of the PVA/GO composite film at 323 °C was due to the elimination of residual acetate groups, which were on the PVA for the incomplete alcoholysis of poly(-vinyl acetate). However, for the PVA/GO/$CuSO_4{\cdot}5H_2O$ composite films, the maximum heat loss rate occurred at temperatures of about 230 and 440 °C. At 230 °C, the peaks at 1516 and 1700 cm^{-1} were ascribed to the stretching vibrations of C—C and C═O, respectively. The absorption peak at 3740 cm^{-1} was attributed to the stretching vibrations of hydroxyl groups

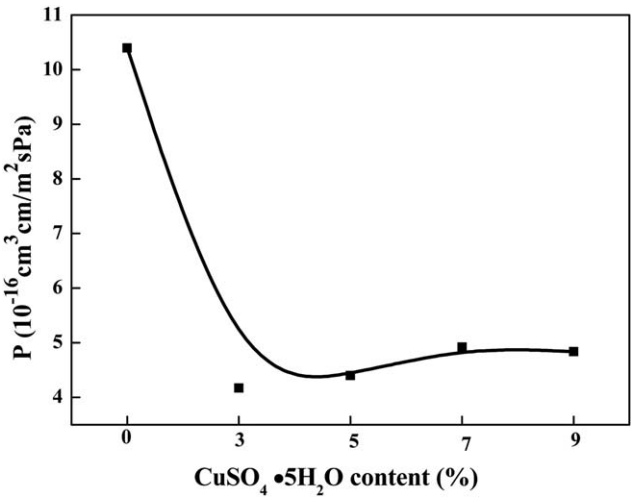

Figure 8. Oxygen-barrier properties of the PVA/GO/$CuSO_4$·$5H_2O$ composite films (P = permeability coefficient of the films).

(—OH). We concluded that the maximum heat loss of the PVA/GO/$CuSO_4$·$5H_2O$ composite film at 230 °C was due to the release of the glycerol plasticizer present in PVA and the elimination of tiny amounts of residual acetate groups. At 440 °C, the peaks at 2930 and 1730 cm^{-1} were assigned to the stretching vibrations of C—H and C═O, respectively. The results demonstrated that the mass loss at 440 °C was attributed to the breakdown of the polymer backbone. We concluded that the introduction of Cu^{2+} promoted the decomposition of oxygen functional groups; this indicated a decrease in the thermal stability of the PVA/GO composite film.

Gas Permeability

The oxygen-barrier properties of the PVA/GO/$CuSO_4$·$5H_2O$ composite films is shown in Figure 8. With the introduction of $CuSO_4$·$5H_2O$, the O_2 permeability coefficient of the composite films decreased by 67% for the composite film with 3% $CuSO_4$·$5H_2O$ compared with the neat PVA/GO composite film; this indicated a remarkable improvement in the barrier properties. When the content of $CuSO_4$·$5H_2O$ was higher than 3%, the O_2 permeability coefficient was almost unchanged. Generally, gas permeation through a PVA membrane is explained by the solution–diffusion model. GO was a two-dimensional honeycomb lattice material with a unique layer structure on the nanometer scale. The layer structure of GO was dispersed well in the PVA matrix. When the film was formed, these layers became the main barrier in the composite film for preventing the oxygen gas from passing through and, thus, extended the length of the passing path for the oxygen to penetrate. The crosslinking effect of interactions between the hydroxyl groups of PVA and Cu^{2+} ions and the increase in the crystallinity of the films reduced the free volume of the PVA molecular chain and decreased the flexibility of the PVA chains; this also brought about an improvement in the gas-barrier properties. Overall, with the addition of $CuSO_4$·$5H_2O$ into the PVA/GO composite films, the oxygen-barrier properties of the PVA/GO/$CuSO_4$·$5H_2O$ composite films were greatly improved.

CONCLUSIONS

PVA/GO/$CuSO_4$·$5H_2O$ composite films were prepared with the solution casting method. FTIR analysis proved the crosslinking interaction between $CuSO_4$·$5H_2O$ and the —OH group of PVA. The crystallinity of the composite films increased first; this was followed by an insignificant change. For the composite films, the tensile strength, Young's modulus, and yield stress were improved with increasing $CuSO_4$·$5H_2O$ content, whereas the elongation at break of the composite films decreased compared with that of the neat PVA/GO composite film. The TGA and DTG patterns of the PVA/GO/$CuSO_4$·$5H_2O$ composite films showed that the thermal stability was decreased. In addition, a remarkable improvement in the oxygen-barrier properties was achieved. The oxygen permeability coefficient was reduced by 67% compared to that of the neat PVA/GO composite film. Thus, the PVA/GO/$CuSO_4$·$5H_2O$ composite films showed excellent mechanical and barrier performance with the incorporation of $CuSO_4$·$5H_2O$.

ACKNOWLEDGMENTS

This work was supported by the National Natural Science Foundation of China (contract grant numbers 51373004 and 51203004), the Innovation Ability Promotion Plan of the Beijing Municipal Commission of Education contract grant number (PXM2013_014213_E000097), the Beijing Top Young Innovative Talents Program (contract grant number 2014000026833ZK13), and the Key Laboratory for Solid Waste Management and Environment Safety Open Fund (contract grant number SWMES 2013-08).

REFERENCES

1. Valentina, G.; Alina, M. H.; Florin, I.; Gabriel, S.; George, D. M.; Alexandru, M. G.; Anton, F. *Appl. Surf. Sci.* **2014**, *306*, 16.
2. Alexandre, R. B.; Renata, F. M. O.; Paula, M. J.; Nicolás, A. R.; Roberto, R. A. *Micropor. Mesopor. Mater.* **2014**, *185*, 86.
3. Han, Y. Q.; Lu, Y. *Compos. Sci. Technol.* **2009**, *69*, 1231.
4. Liu, P. G.; Gong, K. C.; Xiao, P.; Xiao, M. *J. Mater. Chem.* **2000**, *10*, 933.
5. Xu, J.; Hu, Y.; Song, L.; Wang, Q.; Fan, W.; Chen, Z. *Carbon.* **2002**, *40*, 450.
6. Verdejo, R.; Bujans, F. B.; Rodriguez-Perez, M. A.; Sajab, J. A.; Lopez-Manchado, M. A. *J. Mater. Chem.* **2008**, *18*, 2221.
7. Du, X.; Yu, Z. Z.; Dasari, A.; Ma, J.; Mo, M.; Meng, Y.; Mai, Y. W. *Chem. Mater.* **2008**, *20*, 2066.
8. Yang, Y.; Wang, J.; Zhang, J.; Liu, J.; Yang, X.; Zhao, H. *Langmuir* **2009**, *25*, 11808.
9. Wang, X.; Jin, J.; Song, M. *Eur. Polym. J.* **2012**, *48*, 103.
10. Wu, X. Y.; Huang, S. W.; Zhang, J. T. *Macromol. Biosci.* **2004**, *4*, 71.
11. Li, Y.; Tian, H. F.; Jia, Q. Q. *J. Appl. Polym. Sci.* **2015**, *132*, 46.
12. Lee, J. S.; Choi, K. H.; Do, G. H. *J. Appl. Polym. Sci.* **2004**, *93*, 4.

13. Wu, W. Q.; Tian, H. F.; Xiang, A. M. *J. Polym. Environ.* **2012**, *20*, 63.
14. Hou, Y.; Tang, J.; Zhang, H. B.; Qian, C.; Feng, Y.; Liu, J. *ACS Nano* **2009**, *3*, 1057.
15. Tan, Y. Q.; Song, Y. H.; Zheng, Q. *Chin. J. Polym. Sci.* **2013**, *31*, 399.
16. Zhao, X.; Zhang, Q. H.; Hao, Y. P.; Li, Y. Z.; Fang, Y.; Chen, D. J. *Macromolecules* **2010**, *43*, 9411.
17. Cho, M. J.; Park, B. D. *J. Ind. Eng. Chem.* **2011**, *17*, 36.
18. Prasad, K. E.; Das, B.; Maitra, U.; Ramamurty, U.; Rao, C. N. R. *Proc. Natl. Acad. Sci. U.S.A.* **2009**, *106*, 13186.
19. Zhu, J.; Zhang, H.; Kotov, N. A. *ACS Nano* **2013**, *7*, 4818.
20. Li, J.; Shao, L.; Yuan, L.; Wang, Y. *Mater. Des.* **2014**, *54*, 520.
21. Chen, D.; Wang, X. Y.; Liu, T. X.; Wang, X. D.; Li, J. *ACS Appl. Mater. Interfaces* **2010**, *2*, 2005.
22. Ye, Y. S.; Cheng, M. Y.; Xie, X. L.; Rick, J.; Huang, Y. J.; Chang, F. C.; Hwang, B. J. *J. Power Sources* **2013**, *239*, 424.
23. Yang, X. M.; Li, L. A.; Shang, S. M.; Tao, X. M. *Polymer* **2010**, *51*, 3431.
24. Wang, Y.; Yang, H.; Xu, Z. *J. Appl. Polym. Sci.* **2008**, *107*, 1423.
25. George, J.; Sajeevkumar, V. A.; Ramana, K. V.; Sabapathy, S. N. *J. Mater. Chem. A* **2012**, *22*, 22433.
26. Qi, X.; Yao, X.; Deng, S.; Zhou, T.; Fu, Q. *J. Mater. Chem. A* **2014**, *2*, 2240.
27. Bian, Q. B.; Tian, H. F.; Wang, Y. R.; Liu, Q.; Xiang, A. M. *Polym. Sci. Ser. A* **2015**, *57*, 836.
28. Wang, J.; Xiang, A. M. *J. Polym. Mater.* **2009**, *26*, 267.
29. Abdol, R. H.; Fatemeh, M.; Mohammad, R. S. *J. Phys. Chem. Solids* **2015**, *83*, 96.